NEU PRESS

FIVE ZERO

Volume: 5 Issue: 1 Year: 2025 Research Article e-ISSN: 2578-8965

Diabetic Retinopathy and Glaucoma Diagnosis with CNN-Based Approach and User Interface for Morphological Analysis of Risky Regions in Fundus Images

Saim ERVURAL[1*] Emre ERGÜLER[2] Mehmet Akif TOKEL[2]

[1] KTO Karatay University, Faculty of Engineering and Natural Sciences, Electrical, Electronics Engineering Department, Konya, Türkiye

[2] KTO Karatay University, Konya, Türkiye

Article Info

Received: 13.11.2024
Accepted: 04.06.2025
Published: 30.06.2025

Keywords:
Diabetic retinopathy,
optic disc,
machine learning,
ımage processing.

ABSTRACT

Early diagnosis and effective monitoring of diabetic retinopathy and glaucoma are essential for preventing vision loss and improving patient outcomes. These conditions, if detected early, can be managed effectively, reducing the burden on healthcare systems and improving quality of life for patients. This study presents the development of a user-friendly software interface designed to assist healthcare professionals in diagnosing these conditions more efficiently. We developed a custom 11-layer Convolutional Neural Network (CNN) architecture, beginning with a rescaling layer and incorporating data augmentation techniques. The primary architecture consists of three convolutional layers containing 16, 32, and 64 filters, respectively, each followed by max pooling layers. A dropout layer with a 0.7 rate was incorporated to reduce the risk of overfitting. The network also features a flattening layer, a dense layer with 128 neurons for feature extraction, and an output layer tailored to the number of classes. For glaucoma detection, a specialized preprocessing step focusing on the optic disc reduced validation loss by approximately 20%. Additionally, a manual zooming feature was developed to enhance diagnostic accuracy in complex glaucoma cases. The algorithms for diabetic retinopathy were meticulously designed to identify and highlight pathological areas, such as edema and hemorrhage. This approach facilitates precise visualization of vascular structures and significantly enhances the model's capability to provide accurate and timely diagnoses. The architecture that emerged upon conclusion of the study demonstrated an accuracy of 98% for diabetic retinopathy and 85% for glaucoma. This study highlights the potential of advanced deep learning combined with practical tools to improve diagnostics, offering clinicians a reliable system to enhance patient outcomes.

Fundus Görüntülerinde Riskli Bölgelerin Morfolojik Analizi için CNN Tabanlı Yaklaşım ve Kullanıcı Arayüzü ile Diabetik Retinopati ve Glokom Teşhisi

Makale Bilgisi

Geliş Tarihi: 13.11.2024
Kabul Tarihi: 04.06.2025
Yayın Tarihi: 30.06.2025

Anahtar Kelimeler:
Diabetik retinopati,
optik disk,
makine öğrenimi,
görüntü işleme.

ÖZET

Diyabetik retinopati ve glokomun erken teşhisi ve etkili yönetimi, görme kaybının önlenmesi ve hasta sonuçlarının iyileştirilmesi için çok önemlidir. Bu rahatsızlıklar erken teşhis edildikleri takdirde etkili bir şekilde yönetilebilir, sağlık sistemlerinin yükü azaltılabilir ve hastaların yaşam kalitesi iyileştirilebilir. Bu çalışma, sağlık profesyonellerine bu hastalıkların teşhisinde daha verimli destek sağlamak üzere geliştirilen kullanıcı dostu bir yazılım arayüzünü tanıtmaktadır. Çalışmada, 11 katmanlı özel bir Konvolüsyonel Sinir Ağı (KSA) mimarisi tasarlanmıştır; bu yapı, bir yeniden ölçekleme katmanıyla başlayarak veri artırma tekniklerini içermektedir. Temel yapı, sırasıyla 16, 32 ve 64 filtre içeren üç konvolüsyon katmanı ve bunları takip eden maksimum havuzlama katmanlarından oluşurken, aşırı öğrenmeyi önlemek için %0.7 oranında bir dropout katmanı eklenmiştir. Ayrıca ağda, özellik çıkarımı için 128 nöronlu bir yoğun katman ve sınıf sayısına göre uyarlanmış bir çıktı katmanı da bulunmaktadır. Glokom tespiti için optik disk üzerine odaklanan özel bir ön işleme adımı doğrulama kaybını yaklaşık %20 oranında azaltmış, karmaşık glokom vakalarında tanısal doğruluğu artırmak için manuel bir yakınlaştırma özelliği geliştirilmiştir. Diabetik retinopati için ise, ödem ve kanama gibi patolojik alanları tanımlayıp vurgulayan özel algoritmalar tasarlanmış; böylece damar yapılarının hassas bir şekilde görselleştirilmesi sağlanarak modelin doğru ve zamanında teşhis sağlama kapasitesi önemli ölçüde artırılmıştır. Sonuç olarak ortaya çıkan mimari, diabetik retinopati için %98, glokom için ise %85 doğruluk oranına ulaşmıştır. Bu çalışma, tanılamayı iyileştirmek için pratik araçlarla bir araya getirilen gelişmiş derin öğrenmenin potansiyelini vurgulamakta ve klinisyenlere hasta sonuçlarını iyileştirmek için güvenilir bir sistem sunmaktadır.

To cite this article:

Ervural, S., Ergüler, E., & Tokel, M. A. (2025). Diabetic Retinopathy and glaucoma diagnosis with CNN-based approach and user ınterface for morphological analysis of risky regions in fundus images. *Fivezero, 5*(1), 22-44. https://doi.org/10.54486/fivezero.2024.43

***Sorumlu Yazar:** Saim ERVURAL, *saim.ervural@karatay.edu.tr*

INTRODUCTION

Diabetic retinopathy and glaucoma are common ocular conditions with significant implications for vision. Diabetic retinopathy is a consequence of prolonged hyperglycemia, which results in damage to the retina in individuals with diabetes. Glaucoma, on the other hand, involves the gradual degeneration of the optic nerve, leading to a progressive loss of visual field. This article discusses the core characteristics of these diseases and investigates the capability of Convolutional Neural Networks (CNNs) in their diagnostic processes, aiming to improve detection and management through advanced image analysis.

Diabetic Retinopathy Complication

Diabetes is an endocrine disorder that disrupts glucose metabolism. Under normal physiological conditions, beta cells within the pancreatic islets of Langerhans secrete insulin to regulate glucose levels. Insulin aids in glucose absorption by peripheral tissues and encourages glycogen production in the liver, helping to keep blood glucose levels within a stable range (American Diabetes Association, 2020a; American Diabetes Association, 2020b). While diabetes encompasses several types, focusing on type 1 and type 2 diabetes is particularly pertinent. These types are among the most prevalent causes of diabetic retinopathy and have been widely researched in literature.

Type 1 diabetes is marked by the autoimmune attack on pancreatic beta cells, leading to the complete stop of insulin production. Consequently, individuals that have type 1 diabetes need external insulin therapy (International Diabetes Federation, 2019). Type 2 diabetes, by contrast, is often linked to insulin resistance and impaired function of beta cells. (Centers for Disease Control and Prevention, 2021). Contributing factors include obesity, genetic predisposition, age, and lifestyle (Hu, 2011; McCarthy, 2004; Huang, 2011). Management of type 2 diabetes may involve lifestyle modifications, oral antidiabetic medications, and, if necessary, insulin injections (Centers for Disease Control and Prevention, 2021).

Diabetes manifests with various symptoms, including persistent thirst, frequent urination, fatigue, blurred vision, and slow-healing wounds. If left uncontrolled, severe problems include cardiovascular disease, renal impairment, visual loss, neuropathy, and even limb amputation can result from diabetes. (American Diabetes Association, 2020; World Health Organization, 2016).

Diabetic retinopathy is a prevalent and severe complication impacting vision in diabetic patients. Its pathophysiology involves metabolic disturbances induced by diabetes, which can lead to narrowing, leakage, and even hemorrhage of the retinal blood vessels (Cheung et al., 2016; Antonetti et al., 2006). Treatment strategies for diabetic retinopathy encompass comprehensive diabetes management, pharmacological therapies, laser treatment, and surgical interventions (Yoon et al., 2016). Approximately 40% of individuals with diabetes are expected to develop diabetic retinopathy, highlighting the significant risk of vision loss associated with this condition (Wong et al., 2016). The extent of diabetic retinopathy is strongly correlated with an increased risk of vision loss and blindness, especially in its advanced stages, underscoring the necessity for early detection and effective treatment (Wong et al., 2016; Yau et al., 2012). Globally, the prevalence of diabetic retinopathy aligns with the prevalence of diabetes but varies based on racial and geographical factors. Research indicates that Hispanic and Black Americans face higher risks compared to White Americans in the United States, with similar patterns observed in Asian populations (Wong et al., 2016; Zhang et al., 2010). Additionally, there are disparities in diabetic retinopathy prevalence between countries, with developed nations typically experiencing lower rates of blindness due to effective early diagnosis and treatment services. In contrast, developing countries, where diabetes prevalence is on the rise, tend to report higher rates of blindness (Cheung et al., 2010).

Diabetic retinopathy is primarily classified into two types: Proliferative Diabetic Retinopathy (PDR) and Non-Proliferative Diabetic Retinopathy (NPDR). NPDR indicates the initial stages of the condition, while PDR signifies its advanced stages (Yau et al., 2012). NPDR is additionally divided into moderate, mild, and severe stages, each characterized by increasing severity of microaneurysms, hemorrhages, exudates, and vascular abnormalities observed in fundus images. PDR involves neovascularization and minimal fibrous tissue proliferation in addition to the signs of NPDR (Cheung et al., 2010). Fundus imaging is commonly utilized to detect and evaluate signs of diabetic retinopathy, including microaneurysms, retinal hemorrhages, small vessel changes, and hemorrhagic exudates. Microaneurysms are indicative of early disease stages, while retinal hemorrhages and hemorrhagic exudates are frequently observed in advanced stages, potentially leading to significant vision impairment. Small vessel changes can be detected early, reflecting disease progression. These findings are crucial for diabetic retinopathy diagnosis and treatment using fundus imaging (Bressler et al., 2003; Wilkinson et al., 2003; Early Treatment Diabetic Retinopathy Study Research Group et al., 1991; Klein et al., 1984; Bresnick et al., 1984).

Advancements in medical technology and healthcare services have markedly improved diabetic retinopathy diagnosis and treatment. In the early 1980s, awareness and understanding of diabetic retinopathy began to expand (Aiello, 2003). During this period, detection primarily relied on eye examinations and fundus imaging, with treatment options limited to managing advanced hemorrhages (Klein et al., 1980). The early 2000s saw a pivotal shift with the widespread adoption of digital imaging technology. Digital fundus cameras and retinal scanning devices facilitated earlier detection and monitoring of diabetic retinopathy (Hee et al., 1995).

Glaucoma Complication

Glaucoma is a prevalent ocular disease that can result in optic nerve damage and potential vision loss. It is often linked to increased intraocular pressure (IOP); however, certain forms of glaucoma may occur with normal IOP levels. Glaucoma is a leading cause of avoidable blindness worldwide and can manifest in a variety of clinical ways (Tham et al., 2014; Quigley et al., 2006).

One of the common kinds of glaucoma, open-angle glaucoma generally progresses gradually. This condition is characterized by a dysfunction in the drainage of aqueous humor despite the absence of an obstruction in the eye's drainage channels, leading to increased intraocular pressure (Weinreb et al., 2014; Heijl et al., 2002). Angle-closure glaucoma, in contrast, is less common and typically presents abruptly with symptoms such as sudden eye pain, blurred vision, and redness. It is caused by the angle between the cornea and iris narrowing, leading to a complete blockage of the drainage channels (Foster et al., 2002). Several risk factors contribute to the development of glaucoma, including advanced age, genetic predisposition, elevated intraocular pressure, diabetes, hypertension, and myopia (Leske et al., 1995; Tielsch et al., 1991). People who have a family history of glaucoma are especially at risk. Moreover, glaucoma is more common in certain ethnic groups, including African Americans, Asians, and Hispanics (Racette et al., 2003; Varma et al., 2004). Glaucoma often progresses asymptomatically, and vision loss may be subtle and go unnoticed until the disease has advanced significantly. Consequently, regular eye examinations are essential to detect glaucoma early. Diagnostic methods include tonometry (measurement of intraocular pressure), ophthalmoscopy (examination of the optic nerve), visual field tests, sophisticated imaging methods like OCT (Optical Coherence Tomography) (Kass et al., 2002; Schuman et al., 1995).

The primary objective of glaucoma treatment is to lower intraocular pressure (IOP) through various methods. Pharmacological therapy involves the use of eye drops to manage IOP. Several classes of medications are available, including prostaglandin analogs, carbonic anhydrase inhibitors, alpha

agonists and beta-blockers (European Glaucoma Society, 2017; Heijl et al., 2002). In cases where medication is insufficient, surgical interventions such as laser trabeculoplasty, trabeculectomy, and the use of drainage implants are employed. These procedures aim to enhance the drainage of aqueous humor or reduce its production to achieve a reduction in intraocular pressure (Jay et al., 1988; Gedde et al., 2012).

Key indicators of glaucoma visible in fundus images include thinning of the retinal nervous fiber layer (RNFL), alterations in the optic disc and transformations in the peripapillary region (Quigley et al., 2006; Weinreb et al., 2014). The optic disc is a critical area where glaucoma manifests most noticeably. Cupping of the optic disc, characterized by an increased cup-disc ratio, is commonly observed in glaucoma-affected eyes. As the disease progresses, the ratio between the central depression (cup) and the disc's edge enlarges, signifying a loss of optic nerve fibers (Heijl et al., 2002; Caprioli et al., 2011). Notching at the optic disc margin and displacement of vessels at the disc edge are also indicative of glaucoma (Jonas et al., 1999).

Thinning of the RNFL is a significant diagnostic feature that can be detected even when glaucoma is only getting started. The RNFL, composed of nerve fibers forming the optic nerve, becomes thinner as these fibers are damaged. In fundus images, RNFL thinning is particularly evident around the optic disc. Advanced imaging techniques such as Optical Coherence Tomography (OCT) are utilized to measure RNFL thickness accurately and assess the progression of glaucoma (Schuman et al., 1995; Leung et al., 2010). Glaucoma can also lead to a variety of alterations in the peripapillary area surrounding the optic disc. Peripapillary atrophy, marked by thinning of the choroid and retinal pigment epithelium, is often more pronounced in glaucomatous eyes. In fundus images, peripapillary atrophy is represented as lighter areas surrounding the optic disc (Jonas et al., 1996; Hood et al., 2007).

Diabetic Retinopathy Diagnosis using Fundus Images

Diabetic retinopathy manifests several distinctive signs in fundus images, which are crucial for the management of the condition. These signs include microvascular changes, retinal vascular occlusions, vessel dilations (aneurysms), vessel leaks and exudates, dot hemorrhages, microaneurysms, and optic disc edema (Michaelides et al., 2007; Bandello et al., 2016; Yau et al., 2012).

Microvascular changes: Diabetic retinopathy is characterized by microvascular alterations in retinal vessels. These changes often present as narrowing, dilation, twisting, or a spiral appearance in the vessels. Fundus images reveal these abnormalities as deviations from normal vessel appearance, with microvascular irregularities noted in specific retinal regions.

Retinal vascular occlusions: Occlusions in retinal vessels can occur during diabetic retinopathy, disrupting normal blood flow. Such blockages lead to reduced blood supply in certain areas of the retina. In fundus images, these occlusions are visible as distinct blockages where the vessels appear widened, indicating compromised retinal nutrition.

Vessel dilations (aneurysms): Diabetic retinopathy can cause abnormal dilations of retinal vessel walls due to weakening. These dilations, visible in fundus images, appear as swollen and irregularly shaped vessels.

Vessel leaks and exudates: As the disease progresses, damage to retinal vessels can result in leakage. This leakage leads to fluid accumulation beneath the retina, appearing in fundus images as exudates. Exudates often manifest as yellowish spots or patches on the retina.

These visual signs provide critical diagnostic information and are integral to the effective treatment of diabetic retinopathy (Michaelides et al., 2007; Bandello et al., 2016; Yau et al., 2012).

Diagnosis of Glaucoma in Fundus Images

Glaucoma is a chronic eye condition marked by damage to the optic nerve, frequently linked to elevated intraocular pressure. Fundus imaging is a key tool for monitoring the progression of glaucoma.

Optic nerve atrophy: Glaucoma can lead to degenerative changes at the optic nerve head, observable in fundus images such as pallor, cupping, and signs of optic disc atrophy. Optic nerve atrophy is frequently seen in the advanced stages of glaucoma and may indicate disease progression.

Optic nerve head cupping: Glaucoma can cause a concave shape at the optic nerve. This condition is visualized in fundus images as a loss of the normal optic disc structure or a concave appearance of the optic nerve head. Cupping of the optical nerve head can reflect the severity of glaucoma progression and optic nerve damage.

Retinal vascular changes: Glaucoma can induce alterations in retinal blood vessels. In fundus images, these changes may present as arteriolar narrowing, venous dilation, and twisting of retinal vessels. Such modifications can affect retinal circulation and indicate disease progression.

These results are essential for glaucoma diagnosis and therapy since they show the disease's distinctive symptoms in fundus images. The signs observed in fundus images play an essential role in assessing disease progression and evaluating the response to treatment (Heijl et al., 2002; Johnson et al., 2006; Werner et al., 2007).

MATERIAL AND METHODS

This section details the methodology of the research, outlining the materials used and presenting the structure and fundamental approach.

Data Collection and Annotation

Data for this study was gathered from public databases and several ophthalmology clinics. The initial collection consists of 1,000 fundus images spanning 39 categories, sourced by the Joint Shantou International Eye Center (JSIEC). These images are a subset of a more extensive collection containing 209,494 fundus images, which were used for training, validation, and testing within our DL model (Cen et al., 2021). Additionally, a second collection features approximately 1,000 retinal images per category, including Normal, Diabetic Retinopathy, Cataract, and Glaucoma cases. These images were sourced from repositories such as IDRiD (Indian Diabetic Retinopathy Image Dataset), Ocular Recognition, and HRF (Doddi, n.d.).

Copyright for these images is held by JSIEC. This collection will be employed to develop and evaluate ML algorithms designed for the early diagnosis and classification of eye diseases, including glaucoma and diabetic retinopathy. Healthy fundus images will serve as reference data to establish normative values and enhance model accuracy. The diversity and breadth of these collections enhance the model's ability to generalize and perform effectively across varied populations. This study aims to significantly advance the diagnosis and classification of glaucoma and diabetic retinopathy using fundus images.

Figure 1

The left column shows examples of fundus images from the dataset diagnosed as healthy, the middle column displays examples of fundus images diagnosed with diabetic retinopathy, and the right column presents examples of fundus images diagnosed with glaucoma.

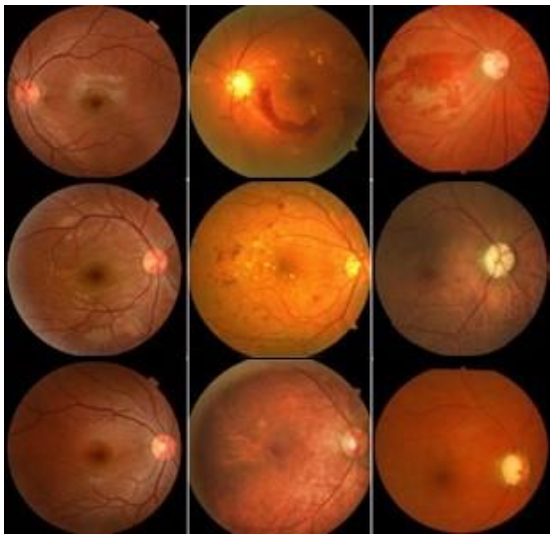

The glaucoma category includes 891 images depicting structural changes such as an increased cup-disc ratio at the optic nerve head, neural retinal rim thinning, and peripapillary atrophy. The diabetic retinopathy category comprises 737 images displaying signs like hard exudates, soft exudates (cotton wool spots), microaneurysms, retinal hemorrhages, and neovascularization, representing various stages of the disease. The healthy fundus images total 916, sourced from individuals without any eye diseases, and are used for normative comparisons.

Table 1

The dataset distribution is illustrated in both percentage and numerical formats based on the categories of fundus images.

Fundus Image Categories	Evaluation Metrics	
	Number of Images	Percent
Diabetic Retinopathy	737	28.96%
Glaucoma	891	35.02%
Healthy	916	36.02%
Total	2557	100%

Deep Learning Algorithm (CNN)

Deep learning involves learning from large datasets through multi-layered artificial neural networks. These models excel in extracting features from data and learning complex relationships. The success of deep learning, particularly with structured data such as images and audio, is attributed to the models' ability to effectively learn complex data relationships when trained on extensive datasets with substantial computational power. CNNs are a type of DL model designed to work efficiently with image data. Each component is crucial for enabling the model to learn features from input data and make accurate inferences.

Convolutional layers perform convolution operations on inputs, extracting feature maps through various filters. These layers identify basic features in images like textures, corners and edges, passing these features to subsequent layers to recognize more complex structures. Filters are trained to detect specific patterns or features, and the output of each filter generates a feature map representing particular aspects of the input image. Pooling layers reduce the dimensions of feature maps and decrease computational load. Max pooling is the most widely used pooling technique, in which the highest value within a defined area is chosen as the representative value for that region. Pooling enhances the model's robustness to spatial variations and reduces computational costs, thereby shortening the training time.

Fully connected layers execute final classification or regression tasks using flattened feature maps. Similar to layers in traditional artificial neural networks, fully connected layers establish connections between all input and output units. These layers integrate the features learned by the model to make final decisions, with the output layer typically generating probability values for specific classes. By integrating these components, CNNs learn hierarchical structures, from low-level features to high-level, within images. This ability allows CNNs to excel in image classification and object detection tasks. The architecture of CNNs facilitates the understanding and interpretation of complex visual data through the careful arrangement and optimization of various layers.

The following provides a comprehensive explanation of each layer within the model and its role in the overall architecture. The model begins with a Rescaling layer. This layer normalizes the pixel values of the input images to a range of 0 to 1. Normalization aids in accelerating the model's learning and producing more stable results. Following the Rescaling layer, a data augmentation layer is applied. Data augmentation entails implementing different transformations on the input images to enhance model generalization. In this model, augmentation techniques include horizontal and vertical flipping, as well as rotations up to 0.2 degrees. These techniques help mitigate overfitting, thereby improving its robustness and generalization capabilities.

The model comprises three convolutional layers. The first convolutional layer employs 16 filters to extract low-level features from the image. The number of filters increases to 32 in the second convolutional layer and 64 in the third layer, allowing the model to capture more complex features. Each convolutional layer utilizes a 3x3 kernel and padding='same', which maintains of the input image’s spatial dimensions. The ReLU is applied in these layers to introduce non-linearity, enabling the to learn complex patterns. Subsequent to each convolutional layer is a max pooling layer. This layer decreases the spatial dimensions, to lower the computational load and emphasize the most crucial features. Max pooling picks the maximum value from each patch of the feature map, thus retaining the most prominent features while reducing dimensionality. This approach enhances the model's efficiency and reduces susceptibility to overfitting. After the third convolutional layer, dropout assists in preventing overfitting by ensuring that the model does not overly depend on any single neuron. It improves the model's generalization ability and performance on unseen data. The multi-dimensional outcome from the pooling and convolutional layers is subsequently transformed into a one-dimensional vector by the Flatten layer. The input for the following dense layers is this vector. Flattening is crucial for transitioning fully connected layers from convolutional layers, which perform the final classification.

The first dense layer contains 128 neurons and utilizes the ReLU activation function to learn complex feature interactions. This layer enhances the model's classification capability by integrating features learned from previous layers. The second dense layer produces the model's final output and is correlated with the number of classes.

The Methodology Section for Diabetic Retinopathy Detection

Data augmentation approaches were used to enhance the effectiveness of models. The training dataset's variety is increased by data augmentation, thereby improving the model's generalization ability. This is particularly valuable when dealing with a restricted number of medical images, as it helps make the model more robust against various image variations. The data augmentation process was implemented using TensorFlow's Sequential API. This process involves applying random transformations to images within the training dataset. Techniques used in this study include horizontal and vertical flipping and random rotation. These transformations introduce variations in image orientations, which improves the model's ability to learn from symmetric changes. Additionally, images were randomly rotated up to 0.2 radians (approximately 11.46 degrees), improving the model's

resistance to rotational fluctuations and enabling it to adjust to various viewing angles.

The data augmentation layer was incorporated immediately following the model's input layer. This setup ensures that during training, each image undergoes a variety of random transformations, as illustrated in Figure 2. This method guarantees that only during training will the model be exposed to enhanced data, while its performance is assessed with original, unmodified data during validation and testing. This is essential for accurately evaluating the model's performance with real-world data.

In conclusion, the application of data augmentation techniques has significantly improved the model's ability to learn changes made to the training dataset and enhanced its generalization capabilities. This advancement is particularly beneficial when working with limited medical imaging data, as it allows the model to more accurately recognize diverse disease symptoms and achieve higher accuracy rates in diabetic retinopathy diagnosis.

Figure 2

The sample outputs of the data augmentation processes are presented. The numbered images correspond to the following: the original output is labeled as 1, the rotated version as 2, the translated version as 3, the horizontally flipped version as 4, the vertically flipped version as 5, and the version flipped both horizontally and vertically as 6.

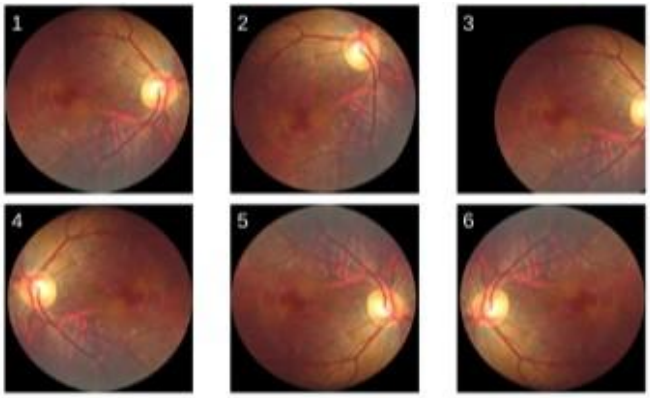

"The Contrast Limited Adaptive Histogram Equalization (CLAHE)" used for further improve the contrast of retinal images to identification. A more sophisticated form of conventional histogram equalization, CLAHE offers localized contrast enhancement, as illustrated in Figure 3. Unlike traditional histogram equalization, which enhances overall contrast by stretching the histogram of the entire image, Through the division of the image into tiny cells, CLAHE enhances local contrast (or tiles) and applying histogram equalization separately to each cell. This method enhances fine details and mitigates noise associated with excessive contrast enhancement.

In this study, the CLAHE parameters were meticulously configured with a clipLimit of 2.0 and a tileGridSize of 8x8. The clipLimit was set to prevent excessive contrast enhancement and mitigate noise, while the tileGridSize ensured the image was divided into smaller cells, facilitating effective local histogram equalization. These parameters were deliberately selected to achieve optimal contrast enhancement while maintaining noise control.

Figure 3

The original photos (left), and the outcomes following the application of histogram equalization (right)

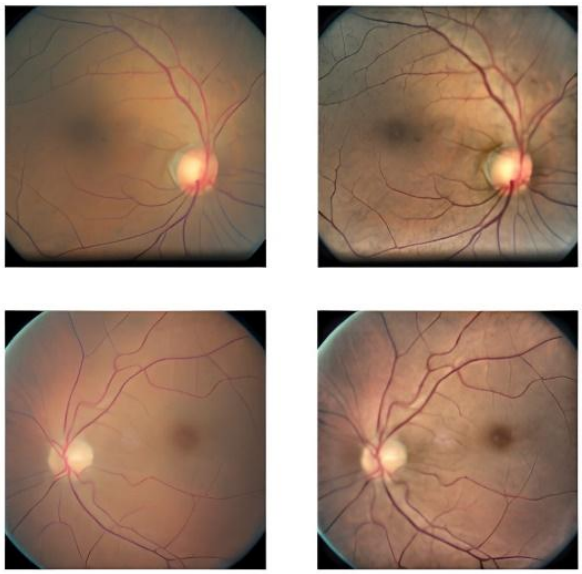

A color space modification was first carried out on the photos before applying CLAHE. Retina images were converted from the BGR (blue-green-red) color space to the LAB (Lightness-a-b) color space. This transformation allows the contrast enhancement process to be applied solely to the lightness component (L), preserving color information and contributing to improved image quality.

In the LAB color space, the image was decomposed into its L, a, and b components, with CLAHE applied exclusively to the lightness component. Enhancing the lightness component with CLAHE improves local contrast, making features such as blood vessels, microaneurysms, and other pathological findings in retinal images more prominent. Following the enhancement, the adjusted lightness component was combined with the original color components (a and b), and the image was reconstructed in the LAB color space before being converted back to the BGR color space. This process effectively increased the contrast of all retinal images, making them more suitable for analysis.

In conclusion, applying the CLAHE method significantly enhanced the contrast of retinal images used for diabetic retinopathy diagnosis, allowing for clearer visualization of pathological findings. This improvement facilitates more accurate and reliable outcomes in clinical diagnosis and treatment. Furthermore, the implementation of CLAHE enhances the performance, contributing to the development of more effective classification and diagnostic models.

The performance of CNN models used in diabetic retinopathy (DR) diagnosis is dependent on proper and consistent preprocessing of input data. Because of the different resolutions of the images in the dataset utilized in this study, it was necessary to resize all images to a uniform dimension. Consequently, all fundus images fed into the CNN model were resized to the smallest image size of 216 x 216 pixels.

The Methodology Section for Diabetic Retinopathy Detection

In this part of the study, we developed an image processing pipeline to detect yellow lesions, indicative of exudates, in fundus. Hard exudates and soft exudates are lipid deposits appearing as yellow spots on the retina, often associated with diabetic retinopathy. Leaking from abnormal blood vessels in the retina, a common diabetic complication, causes these deposits.

Initially, the original fundus image is transformed into a heatmap to enhance visual contrast,

making critical features more distinguishable, as illustrated in Figure 4. CLAHE is then applied with particular focus on the green channel, which is vital in fundus imaging.

Figure 4

The fundus image with the color heatmap is shown.

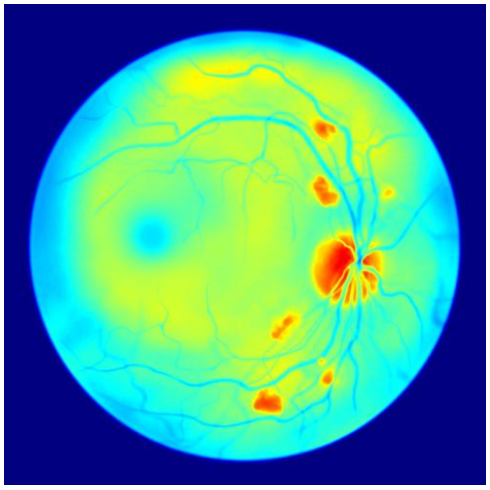

Subsequently, specific color boundaries for yellow and red hues are defined to create masks that isolate these regions within the heatmap. These masked regions are set to black, and the modified heatmap is then converted into a binary image. Contours are detected in this binary image, and an image highlighting these contours in green is generated. These contours are overlaid onto the original fundus image to emphasize the regions of interest.

Further processing involves converting the CLAHE-enhanced image to grayscale and binarizing it. The binary image, which highlights green regions, is then converted back to a colored image and applied to the original image. A transparency effect is applied to the green mask, blending it seamlessly with the original image (Figure 5).

Figure 5

The image shows a fundus image with highlighted exudates.

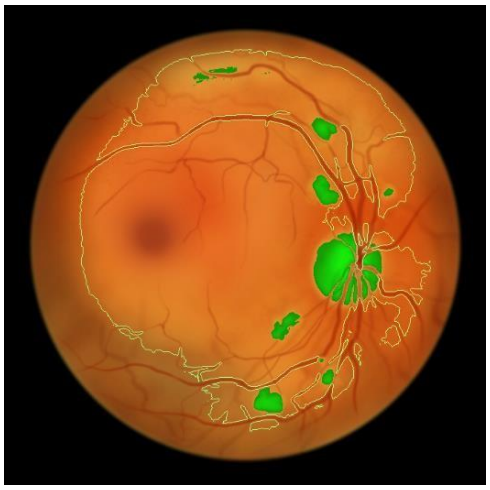

The final processed image displays the highlighted regions, indicating yellow lesions that are crucial for diagnosing diabetic retinopathy. This technique improves fundus image detection and visualization of both soft and hard exudates, providing a powerful instrument for analyzing medical images in relation to diabetic retinopathy. Healthcare providers can more precisely diagnose and track the development of diabetic retinopathy in patients by detecting these lipid deposits.

The Methodology Section for Glaucoma Detection

In this section of the study, the effectiveness and application methods of algorithms used for glaucoma detection are thoroughly examined. These algorithms, developed with machine learning techniques and advanced image processing, analyze various biometric data points. Key data points include intraocular pressure, the retinal layers thickness and the anatomical characteristics of the nerve head, both of which are essential in determining the risk of glaucoma.

To enhance the accuracy of glaucoma diagnosis, this study emphasizes a detailed approach to processing eye images, with particular attention to zooming into specific regions of interest. The process begins with the loading and visualization of a high-resolution color image of the eye. This initial step gives a thorough rundown of the structure of the eye by examining the raw data without any preprocessing. Upon loading the color image, it is converted into grayscale (Figure 6). This conversion eliminates color information, which may be redundant in medical image analysis, leaving only the brightness information. Simplifying the image to grayscale facilitates a more focused examination of structural details by improving the contrast between different components, thus making it easier to identify subtle features.

Subsequent to the grayscale conversion, a median blur filter is applied to the image, achieving the result depicted in Figure 6. This filter reduces noise that could obscure important details and smooths the edges within the image, leading to a more uniform appearance. The reduction of unwanted details through this process enhances the accuracy of the subsequent analysis, ensuring that key features are more clearly visible.

Following the application of the median blur filter, the next step involves detecting circular structures within the eye using the Hough Circle Transform. This technique is effective for identifying prominent circular features, such as the optic disc, as shown in Figure 6.

The algorithm's capability to detect these circular structures is crucial for the precise localization and analysis of critical areas. Among the detected circles, the algorithm identifies the one with the brightest center and marks it on the raw image (Figure 6). This circle is of particular significance as the brightest center typically corresponds to essential structures like the optic disc.

Marking this circle on the original color image ensures that both its center and circumference are distinctly visible. This marking process is integral for further analysis, highlighting regions of interest necessary for diagnosing glaucoma. Enhancing the visibility of these critical structures ensures that the subsequent analysis is both accurate and reliable. This detailed marking assists in the precision of the nerve head, which is essential for evaluating the progression and severity of glaucoma.

Figure 6

The original color image is displayed first (left-up), grayscale counterpart(left-down), the third image in the top right depicts the grayscale image with a median blur filter applied, and the bottom right image highlights the circle detected with the Hough Circle Transform method, emphasizing structures like the optic disc.

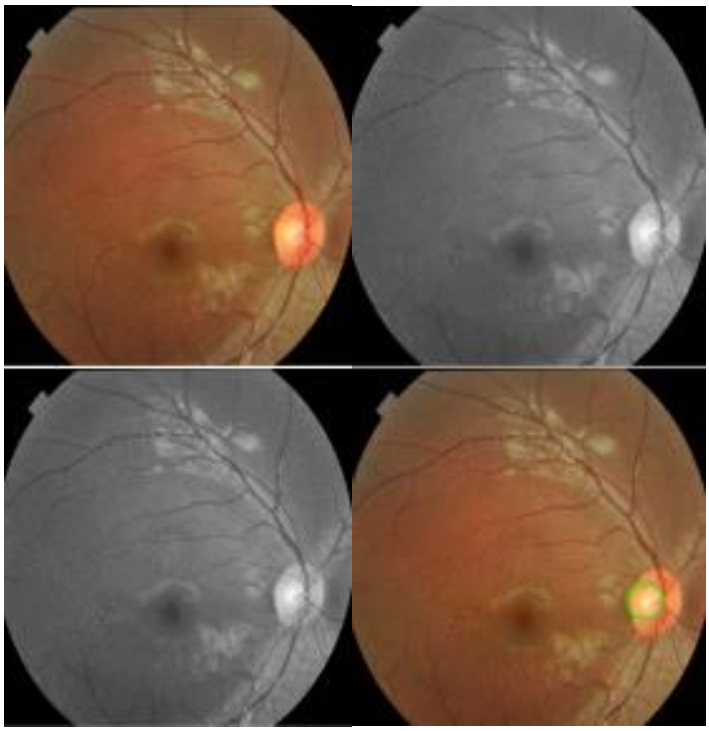

In the final stage, a specific area around the marked circle is enlarged. This process involves focusing on the center of the selected circle and zooming into the surrounding area. Enlarging this region allows for more detailed analysis and better detection of potential abnormalities. The magnified area is subsequently visualized for additional analysis, as illustrated in Figure 7.

Figure 7

Optic disc detection algorithm outputs in images with glaucoma diagnosis.

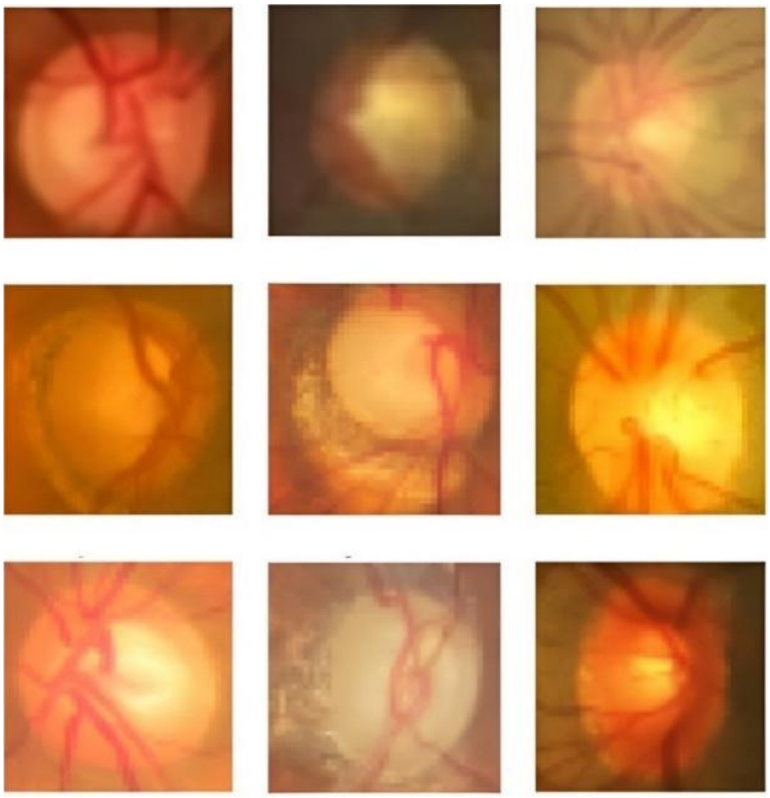

These operations are performed to process and analyze the image in a manner that provides

enhanced data for machine learning models. This process aims to facilitate glaucoma diagnosis and improve accuracy by obtaining high-quality images with distinct features. Consequently, eye disorders such as glaucoma can be diagnosed earlier and with greater precision.

Approach to Optic Disc Evaluation

Due to high noise levels in the processed data, optic disc images that cannot be detected automatically are manually marked by the user. The code scans image files in the specified directory and allows the user to manually intervene with each image. If the images exceed a specified size, they are resized. Users can define a cropping area by drawing a square on the image with the mouse. The square's size can be dynamically adjusted using the mouse wheel. The chosen area is cropped and saved to a specified directory when the left mouse is clicked. During this cropping process, the directory for saving the cropped image is automatically created. The user can exit the process by pressing the "Esc" key or closing the image window. An image is skipped and nothing is done if it has already been cropped. The code also checks for unreadable or faulty files and reports any errors encountered during processing. In conclusion, this application code directory supports the manual inspection of glaucoma-related images, enabling users to select and crop specific areas for further analysis.

EVALUATION METRICS

Using fundus images of individuals with glaucoma and diabetic retinopathy, we methodically assessed the efficacy of many machine learning approaches. The critical role of pre-processing in enhancing model performance was rigorously analyzed using comparative figures and tables, with a focus on learning curves, confusion matrices, and classification reports.

Figure 8

The figure compares learning curves for CNN models trained on original and contrast-enhanced fundus images for diabetic retinopathy detection.

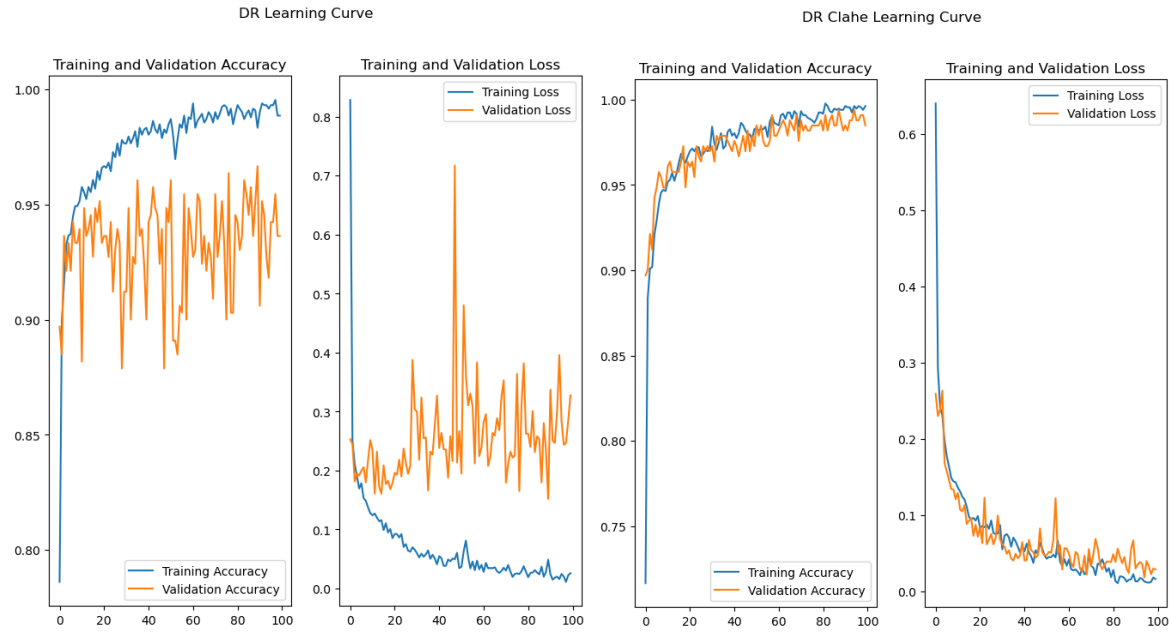

Learning curves were utilized to plot the model's performance, typically measured by error rate or accuracy, against the number of training instances or the duration of training. These curves show how the predicted accuracy of the model increases with the amount of data it is exposed to. The training curve demonstrates the model's performance on the training data, often showing high accuracy initially,

with a potential plateau as additional data is introduced. In contrast, the validation/test curve represents the performance of model's on never seen data, providing insights into its generalization capabilities. This curve typically starts with a higher error rate, which decreases as more training data is incorporated, until it may plateau or diverge, indicating potential overfitting or underfitting.

Learning curves of the CNN model trained with contrast-adjusted fundus images (Figure 8). The training and validation accuracy curves are closely aligned, with only minor deviations, and remain stable at certain points. This alignment indicates that the model performs similarly on both the validation and training, reflecting strong generalization capabilities. The close match between training and validation accuracies suggests that the model has effectively avoided overfitting and has not excessively adapted to the training data. The stability of performance at a certain level signifies that the learning process has been successfully completed and maintained. This consistent performance highlights the model's robustness and its ability to generalize well across different datasets.

Moreover, the convergence of the training and validation curves at a low error rate indicates that the model is operating effectively. This convergence shows how well the model generalizes to new, unknown data and how well it is learned from the training set. Conversely, if the training error is low while the validation error remains high, it would indicate overfitting, suggesting that the on training data, the model works well, but on fresh data, it performs poorly. Conversely, underfitting is observed when both curves exhibit high error rates, indicating that the model is too simplistic to detect the deeper structure in the data. This distinction is crucial for understanding whether the model requires further refinement or if it is appropriately tuned for the given task.

Additionally, contrast adjustments have resulted in noticeable changes in accuracy deviations. When compared to the curves shown in Figure 8, these changes illustrate how varying contrast levels affect the model's performance.

Figure 9

The confusion matrix for diabetic retinopathy shows TP, FP, TN, and FN.

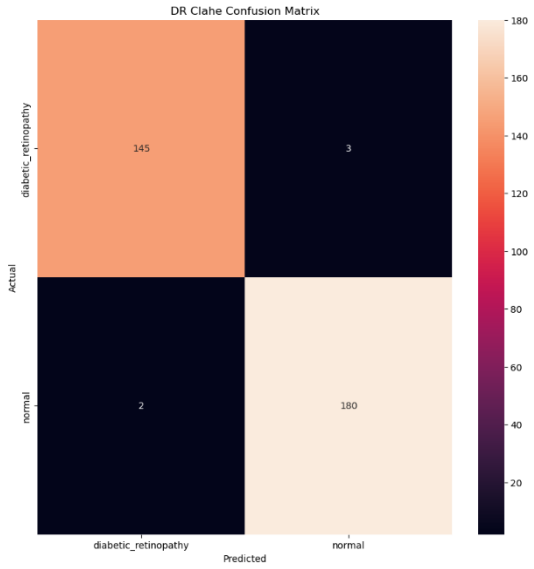

The confusion matrix, a fundamental tool for evaluating classification algorithms, compares the model's predicted labels with the actual ground truth labels from the dataset. This comparison summarizes the model's accuracy in predicting different classes. From the confusion matrix, several critical metrics are derived, including the classification report, which comprises precision, recall, and the F1 score. These metrics can be calculated as shown below.

$$Precision = \frac{TP}{TP + FP}$$

$$Recall = \frac{TP}{TP + FN}$$

$$Precision = 2 \times \left(\frac{Precision \times Recall}{Precision + Recall}\right)$$

These metrics, as seen in Figure 9, demonstrate that the model provides high accuracy and effectiveness, achieving successful performance for both classes. Using the components of this matrix, the performance metrics are calculated as follows: The accuracy of the model is 97.5%, indicating that the model has classified both healthy images and DR cases with high accuracy and demonstrates a strong overall performance. The precision for healthy images is 98.7%, meaning that 98.7% of the cases predicted as healthy are indeed healthy, reflecting a very low FN rate. The recall for healthy images is 98.6%, which means that 98.6% of actual healthy cases have been correctly identified by the model, demonstrating a very low FN rate. The F1 score for healthy images is 98.7%, indicating that the model's predictions for healthy images are well-balanced in terms of both precision and recall. For DR, the precision is 98.9%, showing that 98.9% of the cases predicted as DR are indeed DR, with a very low FP rate. The recall for DR is 98.6%, which means that 98.6% of actual DR cases have been correctly predicted, with a low false negative rate. The F1 score for DR is 98.7%, demonstrating that DR predictions are robust and balanced both precision and recall. Where TP is correctly identified DR cases, and FP is cases incorrectly identified as DR.

Table 2

Table showing the classification performance metrics for diabetic retinopathy and healthy images.

Classification Metrics	DR	Normal	Accuracy
Precision	0.98	0.99	-
Recall	0.99	0.98	-
F1 Score	0.98	0.98	-
Accuracy	-	-	0.98

Table 2 presents classification performance metrics for DR and normal images, including precision, recall, F1-score, and overall accuracy.

In this study, a series of sequential preprocessing steps were applied prior to model training. Techniques such as contrast adjustment, noise reduction, sharpening, and various other methods were employed to enhance image quality. However, it was found that among these steps, contrast adjustment yielded the most significant performance improvement. The other preprocessing steps did not provide the expected contribution and, in some cases, led to undesirable outcomes such as overfitting in the model.

Upon examining the learning curves, confusion matrix, and classification report, it was observed that contrast-enhanced images demonstrated superior generalization ability. This model achieved a 10% higher recall score and a 4% greater accuracy rate in the classification of diabetic retinopathy. Consequently, it was determined that among the various preprocessing steps applied, contrast adjustment played a particularly crucial role in enhancing the model's performance.

Given that the optic disc plays a crucial role in glaucoma detection, we focused exclusively on analyzing the optic disc region within the images for this study. The graphs and tables below demonstrate the improved results of this targeted approach. Learning curves of the CNN model for glaucoma detection (Figure 10), comparing two approaches: training with the original fundus images

versus training with a focus on the optic disc. The upper curve represents the model trained on the original fundus images, while the lower curve shows the model trained with an emphasis on the optic disc. The upper graph demonstrates suboptimal performance, with noticeable deviations and instability in accuracy. In contrast, the lower graph, which focuses on the optic disc, reveals significantly improved performance.

The training and validation curves in the lower graph are closely aligned with minimal deviations, indicating greater stability and accuracy. This suggests that the model, when trained with a focus on the optic disc, generalizes better and detects glaucoma more effectively. The enhanced performance in the lower graph underscores the benefit of focusing on the optic disc, which contributes to a more reliable and robust model for glaucoma detection.

Figure 10

The figure presents two learning curves from CNN models for glaucoma detection. The upper curve depicts the model trained on original fundus images, while the lower curve illustrates the model trained with a close-up focus on the optic disc. This comparison highlights the impact of focusing on the optic disc on model performance.

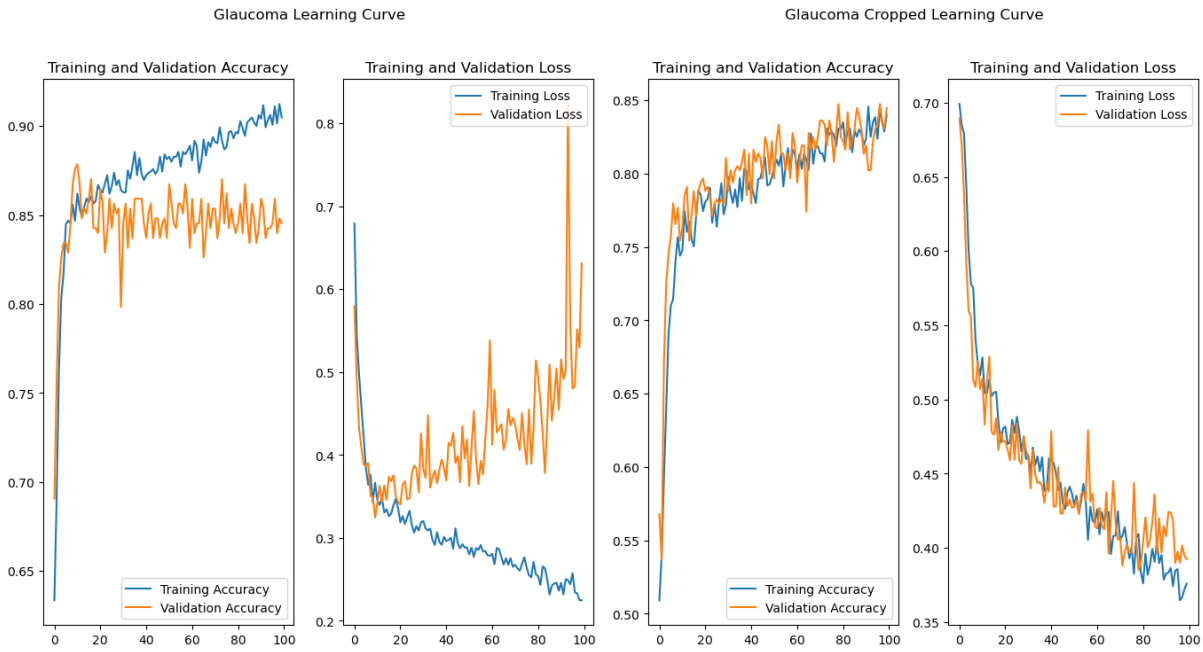

These metrics, as shown in Figure 11, highlight the model's accuracy and effectiveness in detecting glaucoma. The model's accuracy is 83.6%. The precision for glaucoma is 83.4%, indicating that 83.4% of the cases predicted as glaucoma are indeed glaucoma, which reflects a relatively low FP. The recall for glaucoma is 86.2%, meaning that 86.2% of actual glaucoma cases have been correctly identified by the model, demonstrating a relatively low false negative rate. The F1 score for glaucoma is 84.8%, suggesting that the model's predictions for glaucoma are well-balanced. For normal cases, the precision is 82.6%, showing that 82.6% of the cases predicted as normal are indeed normal, with a low false positive rate. The recall for normal cases is 83.8%, meaning that 83.8% of actual normal cases have been correctly predicted, reflecting a low FN. The F1 score for normal cases is 83.2%, indicating that predictions for normal cases are robust and balanced in terms of precision and recall.

Figure 11

The confusion matrix for glaucoma displays true positives, false positives, true negatives, and false negatives.

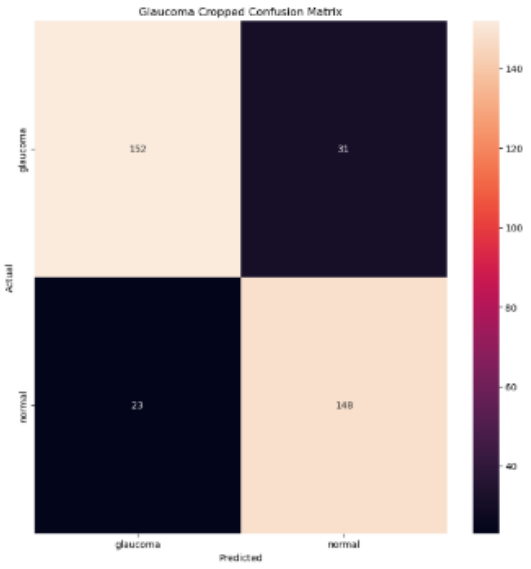

Table 3

Table showing the classification performance metrics for diabetic retinopathy and healthy images.

Classification Metrics	Glaucoma	Normal	Accuracy
Precision	0.83	0.87	-
Recall	0.87	0.83	-
F1 Score	0.85	0.85	-
Accuracy	-	-	0.84

Table 3 summarizes the classification performance metrics for glaucoma and normal images. The metrics include precision, recall, F1 score, and overall accuracy, offering a concise overview of the model's performance for both classes.

RESULTS AND DISCUSSIONS

The results demonstrate that focusing on the optic disc in fundus images of glaucoma patients significantly improved the machine learning model's accuracy. This targeted approach enabled the model to effectively identify the distinctive features of glaucoma within the optic disc, facilitating early detection and diagnosis with high precision. Similarly, preprocessing techniques applied to fundus images of diabetic retinopathy patients, such as image enhancement, noise reduction, and normalization, enhanced the machine learning models' accuracy. These techniques successfully highlighted key pathological features associated with diabetic retinopathy, thus improving the model’s overall performance.

Notably, compared to other models, the architecture used in this work was trained using a lot less data. This suggests that data augmentation could further enhance the model's efficiency and accuracy. In order to investigate possible enhancements in model performance, future research might concentrate on growing the dataset.

Figure 12

The user interface for eye disease detection, which includes tools for uploading fundus images and viewing diagnosis results, is shown.

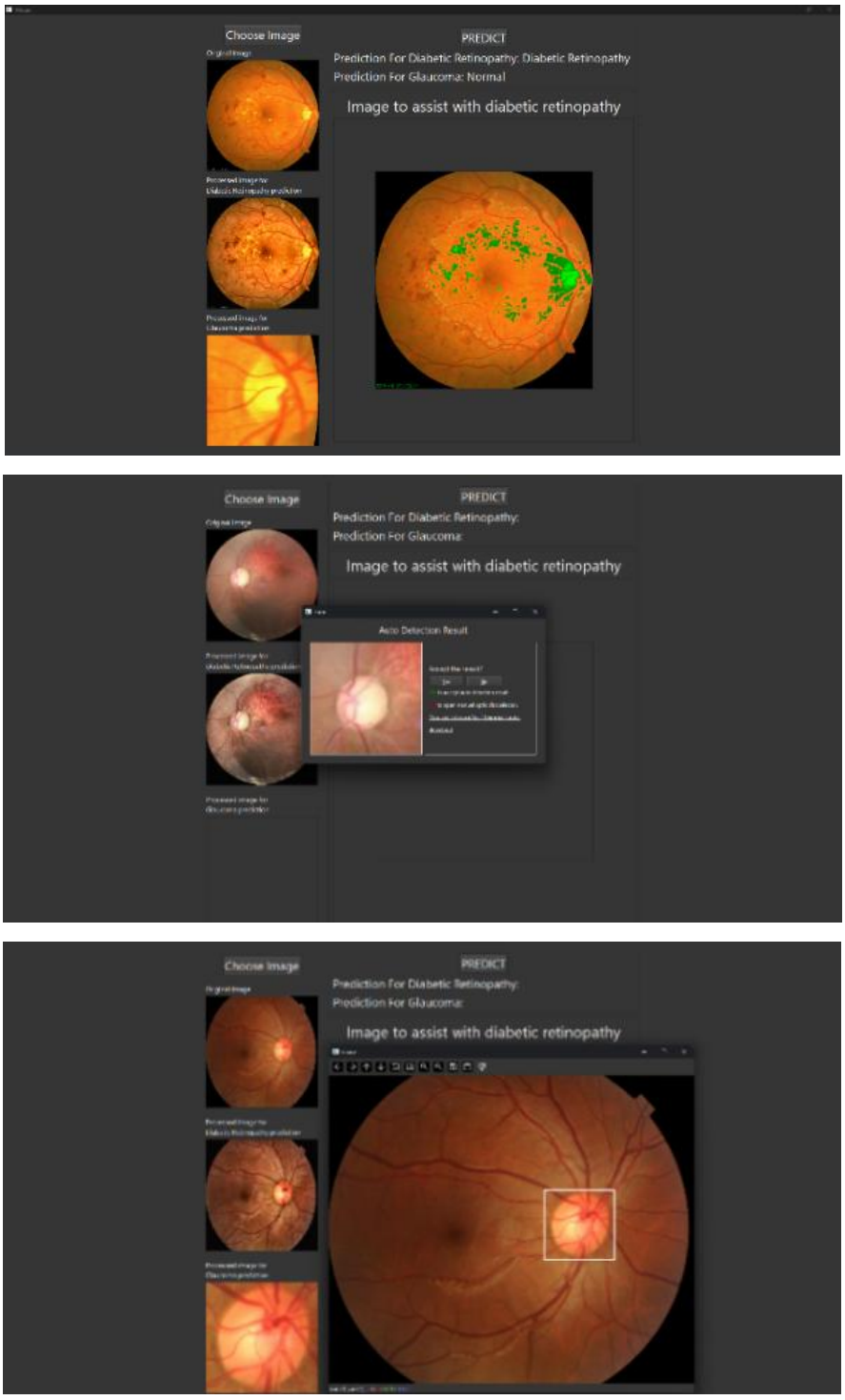

The primary objective of this study was to provide a user-friendly interface for early detection and diagnosis of eye diseases. As shown in Figure 12, the interface facilitates ease of use and accessibility for users, aiming to simplify the diagnostic process. The findings underscore the value of combining appropriate preprocessing techniques with a focus on critical image regions, such as the optic disc, to substantially enhance the effectiveness of machine learning methods in ophthalmology.

In conclusion, the study highlights the importance of precise image processing and targeted analysis in developing robust machine learning models for eye disease detection. These advancements can significantly benefit early diagnosis and management, ultimately improving patient outcomes.

Ethical Approval

It is hereby declared that ethical guidelines have been followed throughout the preparation of this study.

Author Contributions

Research Design Author 1 (%30) - Author 2 (%30) - Author 3 (%40)

Data Collection Author 1 (%10) - Author 2 (%45) - Author 3 (%45)

Research - Data Analysis - Validation Author 1 (%20) - Author 2 (%40) - Author 3 (%40)

Writing the Article Author 1 (%30) - Author 2 (%40) - Author 3 (%30)

Revision and Improvement of the Text Author 1 (%30) - Author 2 (%40) - Author 3 (%30)

Funding

There was no financial support for this study.

Conflict of Interest

The authors declare that there is no conflict of interest.

Sustainable Development Goals (SDGs)

Sustainable Development Goal: **3 Good Health and Well-being**

3.d Strengthen the capacity of all countries, particularly developing countries, for early warning, risk reduction, and management of national and global health risks.

REFERENCES

Aiello, L. P. (2003). Angiogenesis and diabetic retinopathy. *The American Journal of Ophthalmology, 136*(1), 122–135.

American Diabetes Association. (2020a). Diagnosis and classification of diabetes mellitus. *Diabetes Care, 43*(Suppl. 1), S14–S31.

American Diabetes Association. (2020b). Standards of medical care in diabetes. *Diabetes Care, 43*(Suppl. 1), S1–S204.

Antonetti, D. A., Barber, A. J., Bronson, S. K., Freeman, W. M., Gardner, T. W., Jefferson, L. S., ... & Bronson, S. K. (2006). Diabetic retinopathy: Seeing beyond glucose-induced microvascular disease. *Diabetes, 55*(9), 2401–2411.

Bandello, M., et al. (2016). Diabetic retinopathy. *The Lancet, 388*(10050), 1455–1466.

Bresnick, G. H., Condit, R., Syrjala, S., Palta, M., Groo, A., & Korth, K. (1984). Abnormalities of the foveal avascular zone in diabetic retinopathy. *Archives of Ophthalmology, 102*(9), 1286–1293.

Bressler, N. M., Edwards, A. R., Antoszyk, A. N., Beck, R. W., Browning, D. J., Ciardella, A. P., & Ip, M. S. (2003). Retinal thickness on stratus optical coherence tomography in people with diabetes and minimal or no diabetic retinopathy. *American Journal of Ophthalmology, 135*(5), 704–712.

Caprioli, J., & Varma, R. (2011). Intraocular pressure: Modulation as treatment for glaucoma. *American Journal of Ophthalmology, 152*(3), 340–344.

Cen, L. P., Ji, J., Lin, J. W., et al. (2021). Automatic detection of 39 fundus diseases and conditions in retinal photographs using deep neural networks. *Nature Communications*, *12*, 4828.

Centers for Disease Control and Prevention. (2021). *National diabetes statistics report*, *2020*. Atlanta, GA: Author.

Cheung, N., & Wong, T. Y. (2016). Diabetic retinopathy and systemic vascular complications. *Progress in Retinal and Eye Research*, *48*, 8–39.

Cheung, N., Mitchell, P., & Wong, T. Y. (2010). Diabetic retinopathy. *The Lancet*, *376*(9735), 124–136.

Doddi, G. V. (n.d.). Eye diseases classification. Kaggle. https://www.kaggle.com/datasets/gunavenkatdoddi/eye-diseases-classification

Early Treatment Diabetic Retinopathy Study Research Group. (1991). Grading diabetic retinopathy from stereoscopic color fundus photographs—An extension of the modified Airlie House classification. ETDRS report number 10. *Ophthalmology, 98*(5 Suppl), 786–806.

European Glaucoma Society. (2017). *Terminology and guidelines for glaucoma* (4th ed.). Savona, Italy: PubliComm.

Foster, P. J., & Buhrmann, R. (2002). The definition and classification of glaucoma in prevalence surveys. *British Journal of Ophthalmology, 86*(2), 238–242.

Gedde, S. J., Schiffman, J. C., Feuer, W. J., Herndon, L. W., Brandt, J. D., Budenz, D. L., ... & Tube Versus Trabeculectomy Study Group. (2012). Treatment outcomes.

Hee, M. R., Puliafito, C. A., Wong, C., Duker, J. S., Reichel, E., Schuman, J. S., & Fujimoto, J. G. (1995). Quantitative assessment of macular edema with optical coherence tomography. *Archives*

of Ophthalmology, 113(8), 1019–1029.

Heijl, A., Leske, M. C., Bengtsson, B., Hyman, L., Bengtsson, B., & Hussein, M. (2002). Reduction of intraocular pressure and glaucoma progression: Results from the Early Manifest Glaucoma Trial. *Archives of Ophthalmology, 120*(10), 1268–1279.

Hood, D. C., & Kardon, R. H. (2007). A framework for comparing structural and functional measures of glaucomatous damage. *Progress in Retinal and Eye Research, 26*(6), 688–710.

Hu, F. B. (2011). Globalization of diabetes: The role of diet, lifestyle, and genes. *Diabetes Care, 34*(6), 1249–1257.

Huang, E. S. (2011). The natural history of type 2 diabetes: Validating a prognostic model for diabetes progression. *Diabetes Care, 34*(9), 1915–1916.

International Diabetes Federation. (2019). IDF diabetes atlas (9th ed.). Brussels, Belgium: Author.

Jay, J. L., & Murray, S. B. (1988). Early trabeculectomy versus conventional management in primary open angle glaucoma. *British Journal of Ophthalmology, 72*(12), 881–889.

Johnson, C. A., Sample, P. A., Zangwill, L. M., Vasile, C., Cioffi, G. A., Liebmann, J. R., ... & Weinreb, R. N. (2006). The Early Manifest Glaucoma Trial: Overview and baseline characteristics of enrolled patients. *Ophthalmology, 113*(7), 1147–1153.

Jonas, J. B., Budde, W. M., & Panda-Jonas, S. (1999). Ophthalmoscopic evaluation of the optic nerve head. *Survey of Ophthalmology, 43*(4), 293–320.

Jonas, J. B., & Dichtl, A. (1996). Evaluation of the retinal nerve fiber layer. *Survey of Ophthalmology, 40*(5), 369–378.

Kass, M. A., Heuer, D. K., Higginbotham, E. J., Johnson, C. A., Keltner, J. L., Miller, J. P., ... & Gordon, M. O. (2002). The Ocular Hypertension Treatment Study: A randomized trial determines that topical ocular hypotensive medication delays or prevents the onset of primary open-angle glaucoma. *Archives of Ophthalmology, 120*(6), 701–713.

Klein, R., Klein, B. E., Moss, S. E., Davis, M. D., & DeMets, D. L. (1984). The Wisconsin epidemiologic study of diabetic retinopathy. III. Prevalence and risk of diabetic retinopathy when age at diagnosis is 30 or more years. *Archives of Ophthalmology, 102*(4), 527–532.

Klein, R., & Klein, B. E. (1980). Diabetic retinopathy. *Annual Review of Medicine, 31*(1), 219–236.

Leung, C. K., Cheung, C. Y., Weinreb, R. N., Qiu, Q., Liu, S., Li, H., ... & Lam, D. S. (2010). Retinal nerve fiber layer imaging with spectral-domain optical coherence tomography: A prospective analysis of age-related loss. *Ophthalmology, 117*(4), 732–738.

Leske, M. C., Connell, A. M., Wu, S. Y., Hyman, L. G., & Schachat, A. P. (1995). Risk factors for open-angle glaucoma. The Barbados Eye Study. *Archives of Ophthalmology, 113*(7), 918–924.

McCarthy, M. I. (2004). Genetic contribution to type 2 diabetes: Genomic and epidemiologic perspectives. *American Journal of Epidemiology, 159*(12), 1077–1089.

Michaelides, M. B., et al. (2007). Diabetic retinopathy: Pathogenesis, clinical grading, management and future developments. *Diabetic Medicine, 24*(2), 141–150.

Quigley, H. A., & Broman, A. T. (2006). The number of people with glaucoma worldwide in 2010 and 2020. *British Journal of Ophthalmology, 90*(3), 262–267.

Racette, L., Wilson, M. R., Zangwill, L. M., Weinreb, R. N., & Sample, P. A. (2003). Primary open-angle glaucoma in blacks: A review. *Survey of Ophthalmology, 48*(3), 295–313.

Schuman, J. S., Hee, M. R., Puliafito, C. A., Wong, C., Pedut-Kloizman, T., Lin, C. P., ... & Fujimoto, J. G. (1995). Quantification of nerve fiber layer thickness in normal and glaucomatous eyes using optical coherence tomography: A pilot study. *Archives of Ophthalmology, 113*(5), 586–596.

Tham, Y. C., Li, X., Wong, T. Y., Quigley, H. A., Aung, T., & Cheng, C. Y. (2014). Global prevalence of glaucoma and projections of glaucoma burden through 2040: A systematic review and meta-analysis. *Ophthalmology, 121*(11), 2081–2090.

Tielsch, J. M., Katz, J., Singh, K., Quigley, H. A., Gottsch, J. D., Javitt, J., & Sommer, A. (1991). A population-based evaluation of glaucoma screening: The Baltimore Eye Survey. *American Journal of Epidemiology, 134*(10), 1102–1110.

Varma, R., Ying-Lai, M., Francis, B. A., Nguyen, B. B., Deneen, J., Wilson, M. R., & Azen, S. P. (2004). Prevalence of open-angle glaucoma and ocular hypertension in Latinos: The Los Angeles Latino Eye Study. *Ophthalmology, 111*(8), 1439–1448.

Weinreb, R. N., Aung, T., & Medeiros, F. A. (2014). The pathophysiology and treatment of glaucoma: A review. *JAMA, 311*(18), 1901–1911.

Werner, G. K., Sample, P. A., Zangwill, L. M., Vasile, C., Cioffi, G. A., Liebmann, J. R., ... & Weinreb, R. N. (2007). Frequency doubling technology perimetry for detection of visual field progression in glaucoma: A meta-analysis. *Journal of Glaucoma, 16*(2), 117–124.

Wilkinson, C. P., Ferris, F. L. III, Klein, R. E., et al. (2003). Proposed international clinical diabetic retinopathy and diabetic macular edema disease severity scales. *Ophthalmology, 110*(9), 1677–1682. https://doi.org/10.1016/s0161-6420(03)00475-5

Wong, T. Y., Cheung, C. M., Larsen, M., Sharma, S., Simó, R., & Diabetic Retinopathy Barometer Study Group. (2016). Diabetic retinopathy. *Nature Reviews Disease Primers, 2*(1), 1–17.

World Health Organization. (2016). *Global report on diabetes*. Geneva, Switzerland: Author.

Yau, J. W., Rogers, S. L., Kawasaki, R., Lamoureux, E. L., Kowalski, J. W., Bek, T., & Wang, J. J. (2012). Global prevalence and major risk factors of diabetic retinopathy. *Diabetes Care, 35*(3), 556–564.

Yau, L., et al. (2012). Global prevalence and major risk factors of diabetic retinopathy. *Diabetes Care, 35*(3), 556–564.

Yoon, S., Kim, J., & Park, S. (2016). Pathophysiology and therapeutic mechanisms in diabetic retinopathy: Current understanding and future prospects. *Journal of Diabetes Research*, 3789217.

Zhang, X., Saaddine, J. B., Chou, C. F., & Cotch, M. F. (2010). Prevalence of diabetic retinopathy in the United States, 2005–2008. *JAMA, 304*(6), 649–656.

EXTENDED ABSTRACT

Introduction: Early detection and effective monitoring of vision-threatening diseases such as diabetic retinopathy and glaucoma are critical in preventing irreversible vision loss and improving long-term patient outcomes. These conditions, if diagnosed in the early stages, can be managed with appropriate interventions, thereby reducing the burden on healthcare systems and enhancing patients' quality of life. In this context, artificial intelligence and deep learning technologies offer promising opportunities to support ophthalmologists in diagnostic decision-making processes. This study introduces a user-friendly diagnostic software interface integrated with a customized Convolutional Neural Network (CNN) architecture designed to aid in the identification of diabetic retinopathy and glaucoma from retinal fundus images.

Method: An 11-layer CNN model was developed, starting with a rescaling input layer and employing various data augmentation techniques to improve generalization. The core of the model consists of three convolutional layers with 16, 32, and 64 filters, respectively, each followed by max-pooling operations. A dropout layer with a rate of 0.7 was integrated to mitigate overfitting. The feature extraction phase includes a flattening layer and a dense layer with 128 neurons, followed by an output layer tailored to the classification tasks. For glaucoma detection, a targeted preprocessing step focused on the optic disc region led to a 20% reduction in validation loss. Additionally, a manual zooming function was incorporated into the user interface to support expert analysis in diagnostically ambiguous glaucoma cases. For diabetic retinopathy, the model emphasized pathological regions such as edema and hemorrhage to enhance vascular structure visibility and improve diagnostic precision.

Findings: The proposed system achieved an accuracy of 98% for diabetic retinopathy detection and 85% for glaucoma diagnosis. The results show that the CNN model is highly effective in identifying characteristic features of both diseases. The targeted preprocessing strategies and manual interface functionalities contributed significantly to diagnostic performance, particularly in glaucoma cases where optic nerve damage can be subtle. The software also provides real-time visualization of critical pathological areas, which supports clinical decision-making.

Conclusion: This study demonstrates that the integration of deep learning algorithms with user-centric interface design can significantly improve the early detection and management of diabetic retinopathy and glaucoma. The developed system not only provides high diagnostic accuracy but also enhances interpretability through morphological region highlighting, thereby supporting clinicians in delivering timely and precise treatment. The findings suggest that such tools could play a vital role in the future of AI-assisted ophthalmic diagnostics, ultimately improving patient outcomes and reducing preventable vision loss.